Surface modes in plasmonic crystals induced by diffractive coupling of nanoantennas

G. Vecchi,* V. Giannini, and J. Gómez Rivas

Center for Nanophotonics, FOM Institute AMOLF,

c/o Philips Research Laboratories, High Tech Campus 4,

5656 AE Eindhoven, The Netherlands.

(Dated: October 15, 2009)

Abstract

Lattice surface modes in two-dimensional plasmonic crystals of metallic nanoantennas are sustained by the diffractive coupling between localized plasmon resonances. We have investigated experimentally the dispersion of these modes by combining variable-angle transmittance and reflectance spectroscopy. Transmittance spectra through plasmonic crystals reveal quality factors for these modes exceeding 150 in the near infrared, 30 times higher than the quality factor associated to localized plasmon resonances. We have derived the characteristic lengths of the lattice surface modes, distinguishing a regime in which the group velocity is reduced while the mode intensity is strongly confined near the nanoantennas, and a regime in which the surface mode propagates over several unit cells of the plasmonic crystal.

PACS numbers: 73.20.Mf, 42.25.Fx

---

*Electronic address: vecchi@amolf.nl

Metallic nanoparticles have interesting optical properties which are governed by the excitation of localized surface plasmon resonances (LSPRs) [1]. Based on the interplay of the material properties of the nanoparticles and their geometrical design it is possible to make nanoantennas resonant in the visible or near infrared [2]. Several studies have been carried out to investigate the interaction between nanoparticles arranged in 1D and 2D arrays [3–11]. Previous theoretical [9, 10] and experimental [4, 7, 11] work has focused on mode propagation in 1D chains of coupled nanoparticles with a separation much smaller than the wavelength of light, or on arrays of nanoparticles on top of metallic surfaces coupled by surface plasmon polaritons [6], or on arrays of metallic nanostructures coupled by guided modes in dielectric waveguides [5].

In this Manuscript, we provide a detailed analysis of lattice surface modes on plasmonic crystals of nanoantennas. The antennas are coupled through the in-plane scattered light by the array. When LSPRs of nanoantennas in an array are excited, a strong modification in the transmission/extinction characteristics occurs. Of particular relevance is the situation when the distance between nanoantennas and the wavelength of light have similar values. In this case, diffractive coupling due to the scattering of light by the array produces narrow extinction resonances, which have been demonstrated experimentally very recently [12–15]. Such resonances exhibited by arrays of nanoantennas are a signature of the excitation of lattice surface modes extending in the plane of the array. To the best of our knowledge, this Manuscript is the first investigation of the characteristic lengths of lattice surface modes on plasmonic crystals of nanoantennas. We derive the dispersion relation of these modes from variable-angle transmittance measurements. Combining these measurements with reflectance measurements allows deriving the absorbance spectra, provided we restrict this analysis to wavelengths longer than the first diffracted order. We find a maximum in absorbance at the frequencies at which reflection is enhanced and transmission reduced due to the coupling of light to lattice surface modes. From the experimental data we have derived the characteristic lengths of the modes, i.e., the propagation length in the plane of the array and the decay (confinement) length perpendicular to this plane.

We have investigated a 3×3 mm^2 array of gold nanoantennas fabricated by substrate conformal imprint lithography [16] onto an amorphous quartz substrate. A scanning electron microscope image of the array is shown in the inset of Fig. 1(a). The lattice constants are $a_x = 600$ nm and $a_y = 300$ nm along x and y axes, respectively, and the size of the

nanoantennas is $415 \times 85 \times 38$ nm^3. An efficient diffractive coupling between nanoantennas is obtained when the array is embedded in a homogeneous dielectric environment [13–15]. Therefore, we put an amorphous quartz upperstrate on top of the antenna array. Good optical contact between substrate and upperstrate was obtained with a thin layer of refractive index matching liquid. Variable-angle zero-order transmittance and specular reflectance spectra were obtained by illuminating the sample with a collimated beam of white light from a halogen lamp. The polarization was set to probe the localized plasmon resonance associated to the short axis of the nanoantenna, i.e., along the y direction. By changing the angle of incidence on the array in the (x, z) plane, the wave vector component along the x axis was varied. The zero-order transmission, T, and the specular reflection, R, were first measured through/from the array and normalized to the incident light intensity. By energy conservation it is possible to infer the absorbance in the array, A, plus the non-zero order scattering, S, with $A + S = 1 - R - T$. Transmittance and reflectance spectra are shown in Fig. 1(a) for different angles of incidence θ. In the following analysis of the dispersion of lattice surface modes, the transmission through the array of nanoantennas is normalized to the transmission measured across the substrate and upperstrate without nanoantennas. The broad dip of transmittance displayed in Fig. 1(a) around 650 nm corresponds to the excitation of the half-wave localized plasmon resonance of the individual nanoantennas [15]. Fig. 2(a) displays the zero-order transmittance spectra measured as a function of the angle of incidence in the range $6° - 60°$. These measurements are presented as a function of the reduced frequency ω/c and $k_\parallel$, where $\mathbf{k}_\parallel = k_\parallel \hat{x} = k_0 \sin(\theta) \hat{x}$ is the real part of the wave vector component in the plane of the array along the x direction and $k_0 = \omega/c$. In the range of angles of the measurements of Fig. 2(a) the localized plasmon resonance remains nearly unchanged. The other dips in transmittance and peaks in reflectance appearing in the spectra of Fig. 1(a) have a remarkably different dispersive behavior. The dips shift over a broad spectral range while their line width gradually changes as the angle of illumination is varied. These resonances are the result of the coupling of LSPRs of individual antennas with diffracted orders in the array [3, 17, 18]. The vertical lines in Fig. 1(a) correspond to the (1,0) and (-1,0) diffraction edges, calculated at $\theta = 6°$ using $a_x = 600$ nm and the refractive index of the substrate and upperstrate $n = 1.45$. They represent the Rayleigh anomaly conditions at which diffracted orders become evanescent. In particular, the dips in transmittance occur on the long-wavelength side of the corresponding diffraction edge, i.e., at larger wave number

values, which is a signature of coupling of light into an evanescent surface mode [19]. These resonances also display a large contrast in transmittance, particularly under illumination at normal incidence (blue, dotted lines of Fig. 1(a)): in this case, the transmittance switches abruptly from 80% down to 10% within 10 nm. We highlight that these resonances are much narrower than the localized plasmon resonance. The sharpest resonance we have measured has a spectral width at half height of 6 nm, which corresponds to values of quality factor $Q = \lambda/\Delta\lambda \approx 160$ at wavelengths close to 950 nm. This Q factor is much higher than the typical values associated to localized plasmon resonances [1], which in the present case is $Q \approx 6$ at 650 nm. We have fitted the width and wavelength of the resonances with a Fano model [20]. In this model, asymmetric line shapes in the spectrum result from the interference of different pathways for the transmission, namely, a non-resonant contribution arising from the direct transmission and a resonant contribution arising from diffraction in the periodic array. We note that asymmetric Fano line shapes tend to symmetric Lorentzian line shapes when the resonant and non-resonant contribution to the transmission differ substantially, as it is the case in the investigated plasmonic crystals of nanoantennas [21].

Fig. 1(a) points out the correspondence existing between the minima of transmittance and maxima in reflectance. This behavior is verified over a broad angular range by comparing Fig. 2(a) and 2(b), this last showing the results of variable-angle reflectance spectroscopy. The fraction of light neither transmitted in the direction of incidence nor specularly reflected, namely $1 - T - R$, is plotted in Fig. 1(b) as a function of wavelength for $\theta = 6°$ and $10°$. Let us refer to the case of $\theta = 6°$ (black solid line): at wavelengths longer than the (-1,0) diffraction edge in amorphous quartz indicated by the vertical dotted line, i.e., longer than 935 nm, propagating diffracted orders do not exist. In this regime, the narrow maximum of $1 - R - T$ corresponds solely to enhanced absorption. Absorption increases as a result of an enhanced interaction of the electromagnetic field with the lossy metal of the nanoantennas through the coupling to a lattice surface mode [22].

The loci of minima in transmission define the dispersion relation. This dispersion is shown in Fig. 3(a) for the half-wave LSPR and two lattice surface modes. The LSPR is related to the flat dispersion (black squares) around 0.0095 rad nm^{-1} [15]. The dispersion curves of the surface modes are at lower frequencies than the adjacent photon dispersion lines, which represent the Rayleigh anomaly conditions related to the (1,0) and (-1,0) diffractive orders (solid and dashed lines in Fig. 3(a) respectively). Therefore, we label accordingly the modes

4

as (1,0) (red circles) and the (-1,0) (blue triangles). The separation between the Rayleigh anomaly and the lattice surface mode of the same order increases as the frequency approaches the resonance frequency of the LSPR. This observation can be interpreted as a result of the polaritonic character of lattice surface modes arising from the coupling of photonic and plasmonic states. The surface mode dispersion acquires a plasmon-like character as it approaches the LSPR, becoming flatter and its line width broader. At lower frequencies, far from the LSPR, the lattice surface mode acquires a photonic character with a dispersion relation approaching the Rayleigh anomaly.

An important parameter characterizing a surface mode is the propagation length L_x along the surface. Values of L_x of the (1,0) and (-1,0) lattice surface modes are displayed in Fig. 3(b) as a function of wavelength . These values are calculated as $L_x = 1/\Delta k_\parallel$, where $\Delta k_\parallel$ is the full width at half height of the surface mode resonance obtained by fitting the measurements with a Lorentzian. The inset of Fig. 3(b) shows an example of this fit for the wavelength of 851 nm ($\omega/c = 0.00738$ rad nm^{-1}). We obtain values of L_x as high as 15 μm for the (-1,0) surface mode at 970 nm, which means that the surface lattice mode extends over several unit cells of the nanoantenna array. As mentioned above, when the wavelength decreases, the surface mode dispersion approaches the localized plasmon mode and displays an increasingly broad line width, reducing the propagation distance. The highest values of L_x associated to the (1,0) surface mode are limited to ≈ 4 μm at $\lambda = 850$ nm.

The confinement of the electromagnetic field to the plane of the array is defined as the intensity decay length into the surrounding dielectric,

$$L_z = \frac{1}{2Re(\alpha_d)} \, , \tag{1}$$

where α_d is given by

$$\alpha_d^2 = (\tilde{k}_\parallel \pm 2\pi/a_x)^2 - k_0^2 n^2 \, . \tag{2}$$

In Eq. (2) $\tilde{k}_\parallel = k_\parallel + iIm(\tilde{k}_\parallel)$ is the complex in-plane wave vector, the real part $k_\parallel$ being obtained from the dispersion in Fig. 3(a) and the imaginary part $Im(\tilde{k}_\parallel) = 1/2L_x$. Equations (1) and (2) can be applied to single Bloch harmonics in periodic arrays with shallow nanoantennas as those investigated here [23]. The shorter propagation distance L_x of the (1,0) mode corresponds to the stronger field confinement in the z-direction, i.e., shorter L_z. This is illustrated in Fig. 4 by the smaller values of the decay length L_z for the (1,0) surface mode (red circles) compared to the (-1,0) mode (blue triangles). The dependence

of L_z on wavelength indicates that the strongest mode confinement, $L_z = 85$ nm, occurs at wavelengths around 730 nm, when the (1,0) surface mode approaches the localized plasmon resonance of individual nanoantennas. In this regime the mode dispersion flattens due to its localized character, therefore providing the lowest values for the group velocity $v_g = \partial\omega/\partial k_{\parallel} = 0.25c$, obtained by differentiating the dispersion relation. This is illustrated in the inset of Fig. 4, where the group velocity normalized to speed of light in vacuum c is plotted as a function of both the wavelength and the wave vector $k_{\parallel}$.

In conclusion, the interaction between nanoantennas in plasmonic crystals can lead to propagating lattice surface modes. We have determined the dispersion of such modes by variable-angle transmission spectroscopy. Minima of transmittance associated with maxima in reflectance reveal the coupling of light to the modes. Due to the polaritonic character of these lattice surface modes, we can distinguish a photonic-like behavior in which the mode has a high Q factor and propagates over several unit cells of the crystal, and a plasmonic-like behavior corresponding to a reduced group velocity and strong field localization close to the nanoantennas. We note that sharp resonances in systems made of unconnected metallic nanostructures might be of relevance, e.g., for spectroscopic and sensing applications.

---

[1] W. A. Murray and W. L. Barnes, Adv. Mater. **19**, 3771 (2007).

[2] P. Mühlschlegel, H. -J. Eisler, O. J. F. Martin, B. Hecht, and D.W. Pohl, Science **308**, 1607 (2005).

[3] K. T. Carron, W. Fluhr, M. Meier, A. Wokaun, and H. W. Lehmann, J. Opt. Soc. Am. B **3**, 430 (1986).

[4] M. Quinten, A. Leitner, J. R. Krenn, and F. R. Aussenegg, Opt. Lett. **23**, 1331 (1998).

[5] S. Linden, J. Kuhl, and H. Giessen, Phys. Rev. Lett. **86**, 4688 (2001).

[6] N. Félidj, J. Aubard, G. Lévi, J. R. Krenn, G. Schider, A. Leitner, and F. R. Aussenegg, Phys. Rev. B **66**, 245407 (2002).

[7] S. A. Maier, P. G. Kik, H. A. Atwater, S. Meltzer, E. Harel, B. E. Koel, and A. A. G. Requicha, Nat. Mater. **2**, 229 (2003).

[8] S. Zou and G. C. Schatz, J. Chem. Phys. **121**, 12606 (2004).

[9] W. H. Weber and G. W. Ford, Phys. Rev. B **70**, 125429 (2004).

[10] A. F. Koenderink and A. Polman, Phys. Rev. B **74**, 033402 (2006).

[11] K. B. Crozier, E. Togan, E. Simsek, and T. Yang, Opt. Express **15**, 17482 (2007).

[12] V. G. Kravets, F. Schedin, and A. N. Grigorenko, Phys. Rev. Lett. **101**, 087403 (2008).

[13] B. Auguié and W. L. Barnes, Phys. Rev. Lett. **101**, 143902 (2008).

[14] Y. Chu, E. Schonbrun, T. Yang, and K. B. Crozier, Appl. Phys. Lett. **93**, 181108 (2008).

[15] G. Vecchi, V. Giannini, and J. Gómez Rivas, Phys. Rev. Lett. **102**, 146807 (2009).

[16] M. Verschuuren and H. van Sprang, Mater. Res. Soc. Symp. Proc. **1002**, N03-05 (2007).

[17] S. Zou, N. Janel, and G. C. Schatz, J. Chem. Phys. **120**, 10871 (2004).

[18] F. J. García de Abajo, R. Gómez-Medina, and J. J. Sáenz, Phys. Rev. E **72**, 016608 (2005).

[19] H. Raether, *Surface Plasmons* (Springer-Verlag, Berlin, 1988).

[20] U. Fano, Phys. Rev. **124**, 1866 (1961).

[21] C. Genet, M. P. van Exter, and J. P. Woerdman, Opt. Comm. **225**, 331 (2003).

[22] W. L. Barnes, W. A. Murray, J. Dintinger, E. Devaux, and T. W. Ebbesen, Phys. Rev. Lett. **92**, 107401 (2004).

[23] M. Sandtke and L. Kuipers, Phys. Rev. B **77**, 235439 (2008).

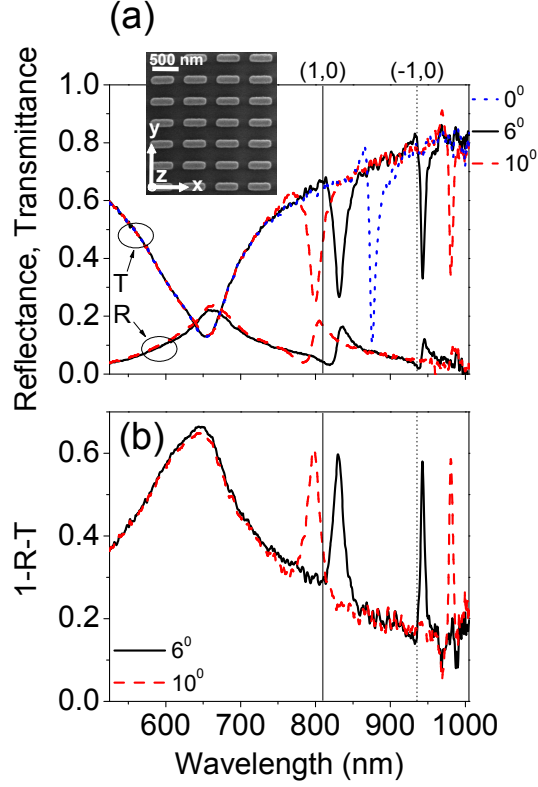FIG. 1: (Color online). (a) Zero-order transmittance, T, through and specular reflectance, R, from a plasmonic crystal of nanoantennas as a function of wavelength for different angles of incidence, $\theta = 6°$ (black solid lines), $\theta = 10°$ (red dashed lines), respectively. Transmittance at normal incidence is shown by the blue dotted line. Light is polarized along the y direction. The wave vector component of the incident wave parallel to the array surface is along the x direction. The vertical solid and dotted lines indicate the (1,0) and (-1,0) Rayleigh anomalies at 6°, respectively. Inset: scanning electron microscope image of a plasmonic crystal of nanoantennas. (b) $1 - R - T$ as a function of wavelength for 6° (black solid line), 10° (red dashed line).
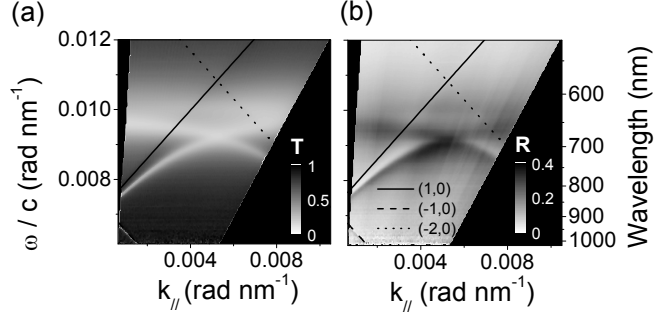
FIG. 2: (a) Zero-order transmittance of light as a function of the normalized frequency ω/c and the wave vector $k_\parallel$. (b) Specular reflectance of light as a function of wavelength and $k_\parallel$. The lines indicate the Rayleigh anomalies in amorphous quartz.
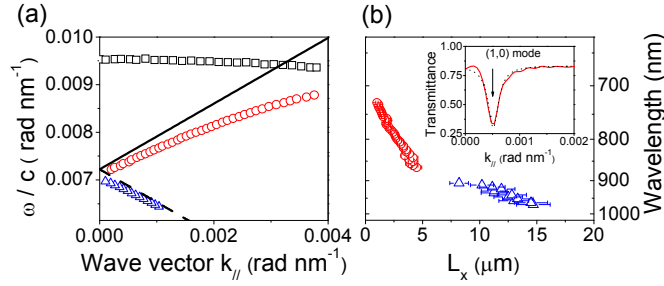

FIG. 3: (Color online). (a) Experimental dispersion relations of the (1,0) and (-1,0) lattice surface modes (red circles and blue triangles, respectively), and of the localized surface plasmon resonance (black squares). The normalized frequency ω/c is plotted versus the parallel wave vector $k_\parallel$. The Rayleigh anomaly associated to the (1,0) and (-1,0) diffraction orders in amorphous quartz is represented by the solid and dashed lines, respectively. (b) Propagation length L_x as a function of wavelength for the (1,0) and (-1,0) lattice surface modes (red circles and blue triangles, respectively). Inset: Transmittance spectrum (red line) and its Lorentzian fit (black dotted line) as a function of $k_\parallel$ at $\omega/c = 0.00738$ rad nm^{-1} ($\lambda = 851$ nm).
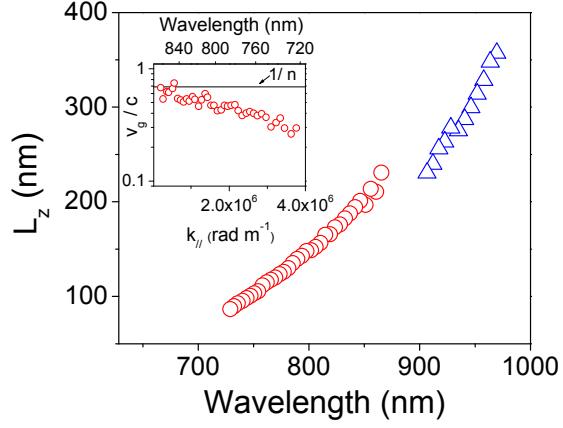
FIG. 4: (Color online). Decay length L_z as a function of wavelength for the (1,0) (red circles) and (-1,0) lattice surface modes (blue triangles). Inset: Group velocity normalized to speed of light in vacuum associated to the (1,0) mode as a function of the wave vector $k_\parallel$ and wavelength. The horizontal line indicates the normalized speed of light in amorphous quartz ($n = 1.45$).